Scanning probes in nanostructure fabrication

Marcus Kaestner, Tzvetan Ivanov, Andreas Schuh, Ahmad Ahmad, Tihomir Angelov, Yana Krivoshapkina, Matthias Budden, Manuel Hofer, Steve Lenk, Jens-Peter Zoellner, and Ivo W. Rangelow[a)]
Department of Micro- und Nanoelectronic Systems, Institute of Micro- and Nanoelectronics, Faculty of Electrical Engineering and Information Technology, Ilmenau University of Technology, P.O. Box 100565, 98684 Ilmenau, Germany

Alexander Reum, Elshad Guliyev, and Mathias Holz
nano analytik GmbH, Ehrenbergstraße 11, 98693 Ilmenau, Germany

Nikolay Nikolov
Microsystems LTD, Chaika 15-D-21, 9010 Varna, Bulgaria

(Received 28 June 2014; accepted 29 September 2014; published 15 October 2014)

Scanning probes have enabled modern nanoscience and are still the backbone of today's nanotechnology. Within the technological development of AFM systems, the cantilever evolved from a simple passive deflection element to a complex microelectromechanical system through integration of functional groups, such as piezoresistive detection sensors and bimaterial based actuators. Herein, the authors show actual trends and developments of miniaturization efforts of both types of cantilevers, passive and active. The results go toward the reduction of dimensions. For example, the authors have fabricated passive cantilever with a width of 4 μm, a length of 6 μm and thickness of 50–100 nm, showing one order of magnitude lower noise levels. By using active cantilevers, direct patterning on calixarene is demonstrated employing a direct, development-less phenomena triggered by tip emitted low energy (<50 eV) electrons. The scanning probes are not only applied for lithography, but also for imaging and probing of the surface before and immediately after scanning probe patterning. In summary, piezoresistive probes are comparable to passive probes using optical read-out. They are able to routinely obtain atomic step resolution at a low thermal noise floor. The active cantilever technology offers a compact, integrated system suited for integration into a table-top scanning probe nanolithography tool. © *2014 American Vacuum Society*. [http://dx.doi.org/10.1116/1.4897500]

I. INTRODUCTION

Routine, "on demand" fabrication of features smaller than 5 nm is a challenge for the realization of many nanoelectronic, nanomechanical, optical or biobased devices. Systems with such low dimension belong to the class of so called "nanosystems," which exhibit peculiar characteristics: quantized excitation,[1,2] a single-atom electron spin qubit in silicon,[3] Coulomb blockade and single-electron tunneling,[4] as well as metal–insulator transition.[5] These phenomena can only occur in structures small enough for quantum mechanical effects to dominate.

Moreover, to extend existing limits in nanodevice manufacturing, new and unconventional lithographic technologies are necessary for novel "beyond CMOS devices." High performance nanometer lithography is an enabling technology therefore.

Scanning probe lithography (SPL) is a thriving area of research in which scanning probe microscopes (SPMs) are used to pattern nanometer-scale features. It offers novel and unconventional means to produce features with single-digit nanometer resolution and unprecedented technical capabilities. This is underpinned by the development of numerous tip-based patterning methods in the last two decades showing the attractiveness and ease-of-use applicability of SPL.

Here, the probe design must meet all the demands for high speed and high resolution SPL. Resolution is determined by the cantilever response to the tip–surface interaction and tip sharpness. Routinely, scanning probes for atomic-force microscopy (AFM) measure surface features with resolution better than 0.01 nm vertically and a few nanometers laterally.

SPL comes in many forms, all of which exploit different interactions between a sharp tip and a surface. Tip/sample interactions can result in a highly confined oxidation, heating, electron exposure, or chemical modification leading to patterning at the nanoscale.[6,7] For example, one approach is to use an electrical bias on the scanning probe tip to generate field emission electrons.[8] The resulting localized electron beam exposes a resist covered sample, like in standard electron beam lithography, but without complex electron beam optics. Hence, high resolution lithography can be accomplished in a table top system.

However, like all maskless patterning techniques, SPL is subject to Tennant's law.[9] That means that throughput goes dramatically down, approximately with the power to five, if resolution is decreased. Throughput enhancement strategies like upscaling of the physical process by active cantilever array technology[10,11] or nanoimprint lithography (NIL) as

[a)]Electronic mail: ivo.rangelow@tu-ilmenau.de

well as the utilization of smart mix-and-match lithographic strategies could overcome these limitations, discussed in more detail in Ref. 12. Despite this trade-off, SPL represents a cost-effective solution for research applications such as rapid nanoscale prototyping.

The first steps toward autonomic cantilevers have already been accomplished using thermal-bimorph cantilevers with an integrated resistive heater.[10] These compact, self-actuating and sensing cantilevers are the basis for parallel probes with 16 × 4 arrays already realized.[13] Overall, four challenges will dictate the viability of SPL as a patterning technology: (1) Probe response for sub-5 nm resolution; (2) tip wear and reliability for hundreds of hours; (3) overlay alignment accuracy better that 1 nm; and (4) desired throughput comparable to electron beam lithography with a Gaussian current density distribution (Gaussian EBL).

The challenge is to maintain the resolution while scanning at speeds needed for high-throughput lithography and metrology. This requires precise and faster detection of the interaction between the sample and the tip. As such, cantilevers must be extremely small and soft with high signal-to-noise ratios (SNR). Ultimately, for production worthy metrology and SPL, probes must be less than 250 nm thick with dimensions of 5 × 12 μm. This is challenging both in terms of fabrication and read-out techniques and requires a new direction in probe design and machining.

The benefit of active cantilevers is the integrated actuation and electrical readout in contrast to expensive and bulky optical based readout. Already today, as presented in this article, the microfabrication technology offers extremely small and soft cantilevers, where optomechanical alignment is challenging or even impossible and, additionally, becomes a drawback with respect to achieving a small size laser spot.

This paper describes the design, characteristics, and challenges of small active and passive cantilever probes for AFM and SPL applications as well as the lithography procedure with the AFM.

II. MINIATURIZATION OF OPTICALLY DETECTED CANTILEVERS

Traditionally in AFM, cantilevers are made from silicon and the displacement is detected by optical laser-based readout. The maximum speed for cantilevers with high SNR is determined by the spring constant, the effective mass, the cantilever damping induced by the surrounding medium (e.g., air or water) and the surface. Standard sized cantilevers are usually too stiff to image at high speeds with high resolution. Herein, a high sensitivity to small forces is required. The simplest method to achieve this is to reduce its geometric dimensions, leading to MHz range resonance frequencies.[14] Using these cantilevers, the authors obtained a sequence of images in liquid at few millisecond intervals.[15] Additionally, high resonant frequencies are needed for rapid adjustment of the vibrating cantilever's amplitude.[16,17] This reduces response time, but can be effectively compensated with an active damping/amplifying circuit.[18] The groundbreaking paper by Viani incorporated all these developments to produce high-bandwidth cantilevers. They showed a high sensitivity and were used to unfold single molecules using pulling speeds an order of magnitude faster than previously performed with conventional cantilevers.[19]

Although revolutionary scanning speeds have been achieved by these developments, the SNR is still an issue for subnanometer resolution lithography and metrology. The ultimate sensing performance of any cantilever is limited by its thermomechanical noise. Low stiffness (<0.01 N/m) cantilevers have enhanced the force sensitivity. However, such cantilevers inherently have a high thermal drift making it difficult to maintain the constant interaction force necessary for high resolution imaging.

If the Z-servo feedback is slow and limited by its bandwidth, the tip may closely approach the sample surface and occasionally touches it. In ambient conditions, most sample surfaces are, in fact, covered with a liquid layer. When a probe tip comes in contact with the sample, the tip may become stuck in this layer due to meniscus forces. In this case, the cantilever oscillation stops. Therefore, when a non-contact AFM (NC-AFM) is operated with very small tip–sample distances, only a slight deviation of the tip–sample interaction force from the set-point can provide a serious tip distortion. This is when the controller of the system is inaccurate and to slow to keep it within the attractive force regime for NC-AFM.

Due to the deposition of a reflective thin metallic film needed for the beam deflection detection, the bimaterial cantilever forms a system that is extremely sensitive to thermomechanical excitations with an SNR of

$$\Delta x/\Delta z = 3/4\sqrt{t_{\text{cantilever}}/2L_{\text{bi–material}}}\,.$$

Ideally, both the thermomechanical noise of the bimaterial cantilever and noise of the readout system should be minimal. We have designed and fabricated cantilevers with low thermomechanical displacement noise.

Silicon-oxide-nitride (SiO_xN_y) cantilever, 245 nm thick, 6 μm long, and 4 μm wide have been routinely fabricated by conventional micromachining batch processes, summarized schematically in Fig. 1. These small cantilevers are coated with titanium/gold and have a resonance frequency above 3 MHz in air and spring constants between 10 and 50 N/m. The power spectral density (PSD) of the small cantilever's thermomechanical fluctuations was compared with standard commercial silicon cantilevers having a similar spring constant, however ~5 μm thick, ~160 μm long, and ~45 μm wide. We employed a small spot laser module with a nominal spot size of 3 × 9 μm and a wave length of 850 nm. The optical detector DC and AC noise was smaller than 5 pm and 25fm · $Hz^{-1/2}$, respectively, at a bandwidth of 7 MHz. The results using optical read-out are summarized in Fig. 2, showing that the thermal PSD [Fig. 2(c)] is one order of magnitude lower for small SiO_xN_y cantilever compared to standard Si cantilever. Figures 2(a) and 2(b) are optical images of the small laser spot focused onto the backside of a standard Si and small SiO_xN_y cantilever, revealing that the application of small passive cantilevers becomes a

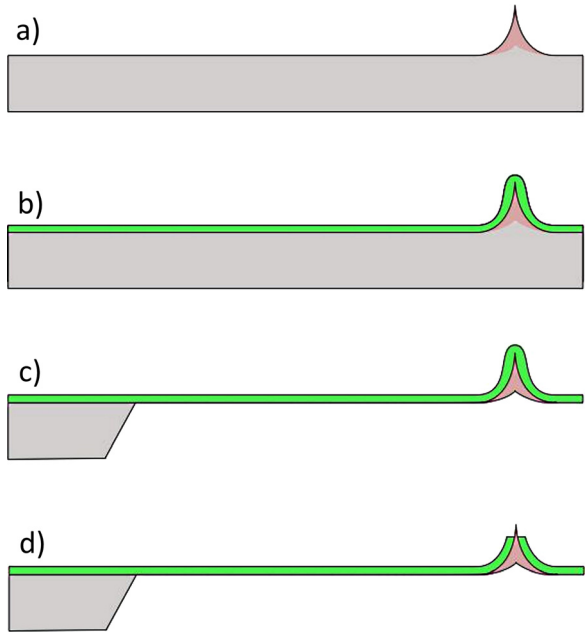

FIG. 1. (Color online) Schematic process flow for fabrication of SiO_xN_y small cantilever: (a) Boron-doped tip formation by optical lithography, plasma etching, and oxidation; (b) low stress deposition of α-Si/SiO_xN_y by PECVD; (c) backside etching; (d) tip opening and release; and (e) reflective coating with Ti/Au.

challenging task using classical optical read-out techniques. By comparing the small laser reflection area of the cantilever (~4 × 6 μm) with respect to the relatively large laser spots of conventional AFMs (~30 μm beam diameter) one can realize the involved challenges. However, in our measurements we have applied the smallest laser spot available for conventional AFM systems (3 × 9 μm), but we are still operating at the limit of the read-out. Thus, for application of further miniaturized passive cantilevers improvements of the laser-based optical read-out are required.

In addition, the conventional optical lever detection technique involves the requirement of optical components and the necessity for their mechanical alignment. When using a top-scanner system like we prefer for our own SPM systems, that fact introduces a lot of engineering challenges and limits the performance of the system, especially for high speed and high precision metrology applications.[20] Thus, cantilever with alternative read-out principles like piezoresistive probes are promising candidates for further miniaturization and improvements, discussed in chapter III.

In Fig. 3(a), a batch-fabricated small SiO_xN_y cantilever with integrated highly boron doped Si tip is shown using SEM. In addition, in the AFM topography image series showing a DNA strand suspended on Mica surface, Figs. 3(b)–3(e), we demonstrate the high speed imaging capability of small high-frequency SiO_xN_y cantilever in amplitude-modulation AFM (AM-AFM) mode. The imaging speed was increased from 10 lines/s at 1024 × 1024 pixel and lines [Fig. 3(b)] of up to 80 lines/s at 128 × 128 pixel and lines [Fig. 3(e)]. Thus, the time required for a full frame AFM image was reduced from 102.4 s [Fig. 3(b)] to 1.6 s [Fig. 3(e)].

The actual development trend of passive probes toward high frequency operation by downscaling of the cantilever dimensions, primarily the length of the cantilever ($f_0 \propto 1/\text{length}^2$), is summarized in Fig. 4. The SEM image series displays selected probe types.

III. COMPACT PIEZORESISTIVE AND SELF-ACTUATED CANTILEVERS

The discovery of the AFM by Binnig[21–23] and its realization by Binnig, Quate, and Gerber[20,22,23] opened up the perspective of surfaces imaging with real atomic resolution. Dynamic modes of atomic-force microscopy offer new possibilities for imaging, because of the availability of the various vibrational modes of the probes. In this case, the cantilever is oscillating at fixed amplitude. The resonance frequency shift in the oscillation amplitude is used as a feedback control to measure the surface topography.

Typically, silicon cantilevers have a relatively high spring constant of 10 N/m and oscillate with amplitudes in the order of 10 nm. We increased the spatial resolution by the

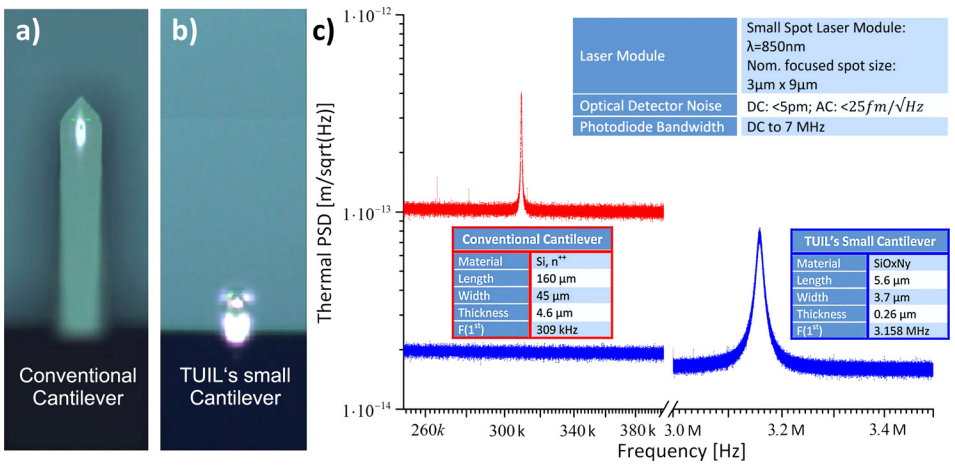

FIG. 2. (Color online) (a) and (b) are optical images of a small laser spot (3 × 9 μm) focused onto the backside of a standard Si and small SiO_xN_y cantilever, respectively. The thermal PSD (c) of both cantilevers was obtained by an average of 1000 samples and a measurement resolution of 4.77 Hz. For thermal PSD measurement, both cantilevers were calibrated by determination of the inverse optical lever sensitivity and spring constant.

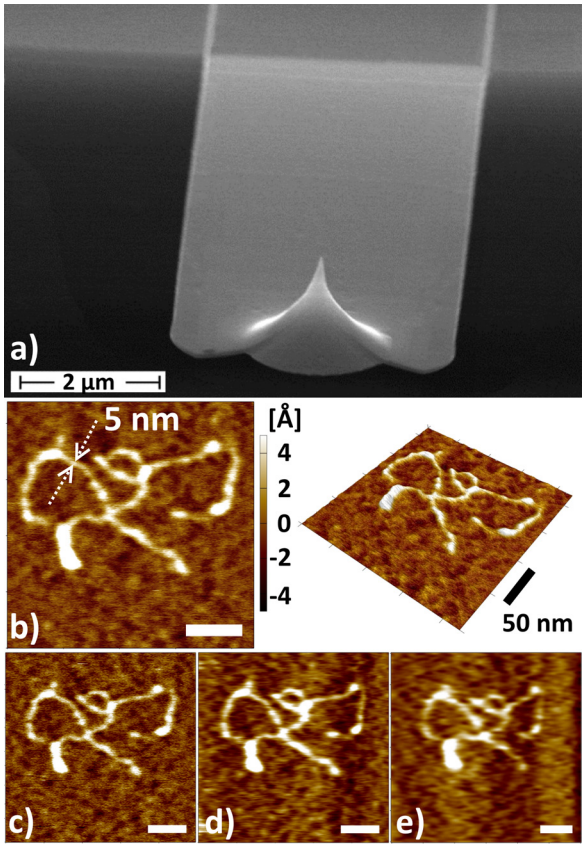

FIG. 3. (Color online) (a) SEM image shows a batch-fabricated 6 μm long and 4 μm wide SiO_xN_y cantilever with integrated highly boron doped 3.5 μm Si tip, coated on the backside with 10 nm Ti and 20 nm Au (scale bar: 2 μm). (b)–(e) AFM topography images of DNA suspended on Mica taken with increased scanning speed to demonstrate the high speed capability of small SiO_xN_y cantilever type (scale bar: 50 nm). AFM imaging was carried out at (b) 1024 × 1024, (c) 384 × 384, (d) 384 × 384, (e) 128 × 128 pixels and lines and (b) 10, (c) 10, (d) 52, (e) 80 lines/s. In summary, the time for a full frame AFM image was decreased from (b) 102.4 s, (c) 38.4 s, (d) 7.3 s, to (e) 1.6 s.

introduction of extremely small self-actuated piezoresistive cantilevers with stiffness in the order of 1 N/m, enabling amplitudes two orders of magnitude smaller that can be used. Here, the cantilever stiffness $k = Ewt^3/4L^3$, where L is the length of the cantilever, w its width and t its thickness, depends on the geometry of the beam as well as its material stiffness.

Piezoresistive readout for atomic resolution AFM imaging was demonstrated for the first time by Tortonese *et al.*[24] in 1993. A significant improvement in the performance of the piezoresistive cantilever with respect to deflection sensitivity was identified using a Wheatstone bridge circuit, with temperature drift compensation noted one year later.[25] Based on this technology, different SPM sensors, such as tribological, thermal and Kelvin-probes were developed.[26] Integration of a sharp tip expanded this MEMS technology into real 3D-micromachining.[27,28] Our active cantilevers are highly integrated and well beyond today's established technology for functional tip arrays. The single probes incorporate actuation and sensing directly onto the cantilever itself, taking advantage of the high performance cantilever fabrication technology that has been developed and demonstrated previously.[10,29–31] A typical active cantilever with aligned tip at the end of the beam is shown in Fig. 5. Two-dimensional electron gas (2DEG) sensors are integrated into the cantilever base.[30] They are thermally isolated from the actuator and designed for minimum electronic crosstalk[31] while being capable of measuring cantilever thermomechanical noise. Integrating a thermally driven bimaterial actuator, in Fig. 5 the meander line on top of the cantilever body, facilitates the development of a scanning probe that is working autonomously with self-oscillating and static bending.[32] By now, the benefit of M(N)EMS technology development has tremendous performance advantages, but with certain exceptions. Aggressive scaling has resulted in the need for low-noise pn-junctions that represents a region of special concern in modern MEMS-Technology. The piezoresistive effect also depends on the temperature.[33] However, the effect of temperature fluctuations on the cantilever read-out signal is routinely reduced using an additional temperature compensation measurement circuit. Piezoresistivity is significantly greater for low dopant concentrations; nevertheless, a high boron (Fig. 5: piezoresistors colored in bright green) implantation dose can be used in order to achieve low temperature dependence.[34] To achieve the optimal force

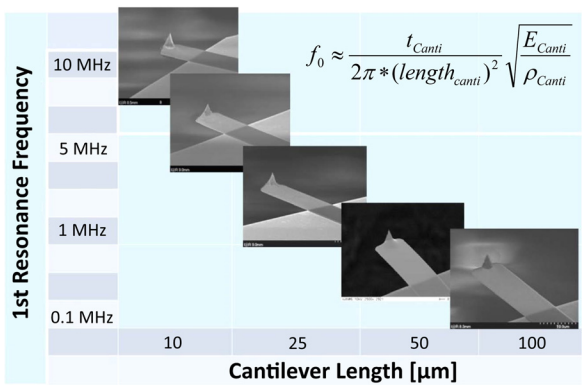

FIG. 4. (Color online) SEM image series outlines the development of small passive cantilevers toward high frequency operation by successive reduction of the cantilever length.

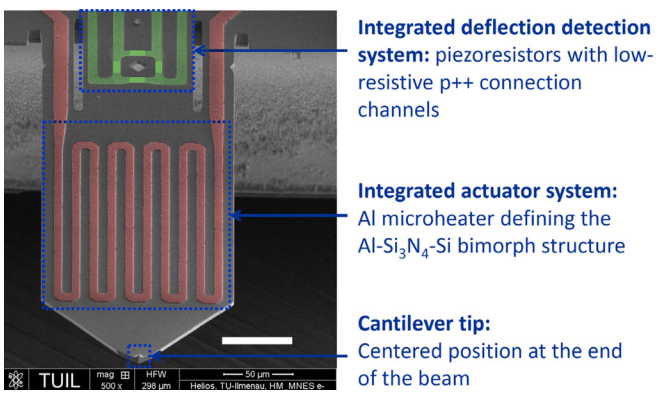

FIG. 5. (Color online) Colored SEM image of an active cantilever with tip at the end of the cantilever beam (scale bar: 50 μm). The thermal bimorph actuator, visible as meander line on top of the cantilever body, as well as the integrated piezoresistors at the base of the cantilever, connected in an integrated Wheatstone bridge configuration, are highlighted respectively.

resolution, the power dissipation needs to be increased to the maximum but still with acceptable drift for the AFM measurements.

The thermomechanical noise floor of our cantilevers equipped with integrated 2DEG sensors operating as piezoresistive read-out was measured with $80\text{fm} \cdot \text{Hz}^{-1/2}$.[35]

Thermally actuated bimorph cantilever with piezoresistive read-out are usually manufactured by bulk micromachining. After formation of the tip by reactive ion etching the electrical shielding lines for sensor–actuator crosstalk suppression are implanted. The piezoresistors (Fig. 5—green) are defined by ion implantation, followed by a thermal annealing step. Subsequently, a silicon nitride layer is formed by PECVD for electrical passivation. On top of that layer a meander-line shaped metal actuator is structured by a lift-off process (Fig. 5—red). Further on, contacts pads for all functional components of the active cantilever are realized. The cantilever thickness is defined by an anisotropic etching step from the backside of the cantilever. Finally, the cantilever is released by a gas chopping etch process.[36,37] Alternatively, cantilevers could also be realized by surface micromachining, SOI-based surface micromachining or polymer-based micromachining. The fabrications processes and their utilization for different types of piezoresistive cantilever are described in more detail in the review article.[31]

In Fig. 6, the development of piezoresistive scanning probes is summarized, revealing a progress toward reduced effective cantilever mass for increased resonance frequency operation. The size of the small piezoresistive cantilever can be easily reduced to 15 μm in length and retain a similar spring constant of 0.021 N/m. We have determined the smallest low frequency force that these cantilevers can detect. A low pass filter at 5 kHz was used and at 1 Hz the standard deviation of the force had a noise level of $11\,\text{pN} \cdot \text{Hz}^{-1/2}$ for the large cantilevers and $6\,\text{pN} \cdot \text{Hz}^{-1/2}$ for the small cantilevers. The thermal motion noise contributed less than 9% to the total noise. The application of SOI-wafers inhibits some of the variations in the spring constant value, which mainly depends on the variation of the cantilever thickness. In this manner, most of the difficulties for

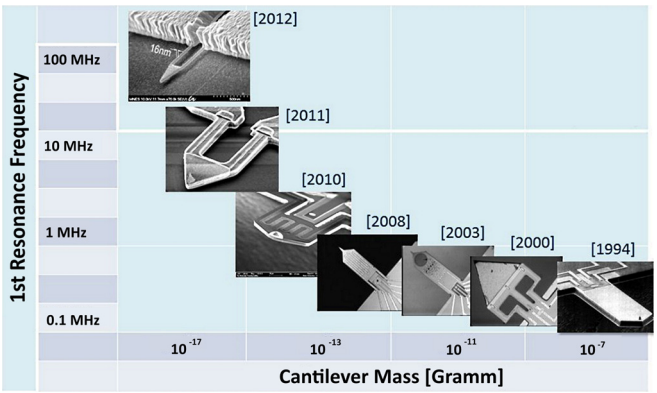

FIG. 6. (Color online) SEM image series summarizes the development of cantilevers with piezoresistive read-out over time. Reprinted with permission from T. Michels and I. W. Rangelow, Microelectron. Eng. **126**, 191 (2014). Copyright 2014, Elsevier.

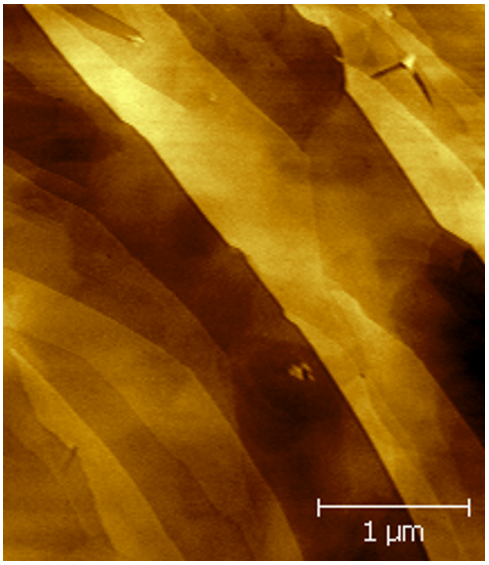

FIG. 7. (Color online) AFM 2D topography image of HOPG indicating single atomic steps obtained at ambient room conditions. The HOPG surface was imaged by a compact thermally actuated active cantilever with piezoresistive read-out.

controlling the cantilever stiffness were overcome.[37,38] We investigated the force resolution of this cantilever in the frequency band of 0.1–1000 kHz and found that it is better than 75 pN. The cantilever sensors are routinely offering atomic step resolution at ambient room conditions. Figure 7 shows an AFM image obtained on highly ordered pyrolytic graphite (HOPG) by an active probe, demonstrating single atomic step resolution of the piezoresistive read-out. In addition, Fig. 8 illustrates four different types of tips that are attached to active cantilevers, such as the ones shown in Figs. 5 and 6. Here, a diversity of different tips tailored for specific applications, for example, for electric field SPL [Figs. 8(a) and 8(d)], is possible.

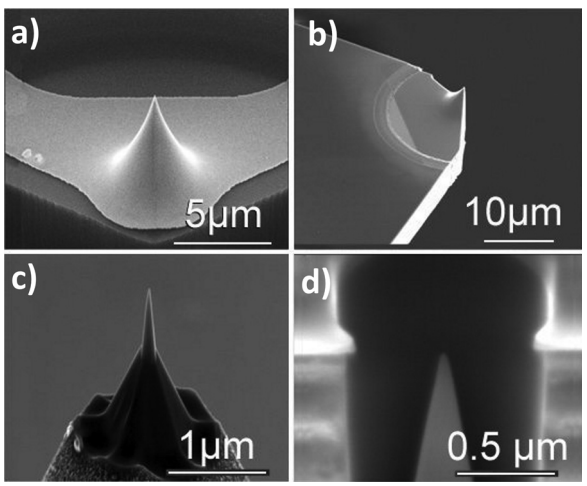

FIG. 8. SEM image series showing different types of cantilever tips applied in AFM and SPL technology, realized on active probes. (a) Metal coated tip for electric field based lithography and Kelvin probe force microscopy; (b) "tip at the edge" type cantilever; (c) focused ion beam sharpened Si tip; and (d) "buried" FN field emission tip for focused electric field, current-controlled SPL.

In addition, active Q-control that changes the actuator signal, based on the current cantilever vibration sensor signal, is applied to these cantilevers in order to modify their dynamic behavior. In contrast with structural changes directly to the cantilever beam, this technique is flexible and the Q-factor can be tuned rapidly and can contribute significantly to the imaging speed. In Fig. 9, a typical frequency sweep of a piezoresistive cantilever, actuated by the thermal actuator, is shown. It includes the total of seven transversal eigenmodes at up to 1 MHz.

Wear is a key factor that hinders the performance of probes for AFM, including AM-AFM mode. Despite the reduced tip–sample interaction compared to contact mode, tip and sample wear can occur through gradual atomic scale processes that can accumulate due to the high frequency of the tip–sample interaction and through high intermittent contact stresses. We are able to select an appropriate probe and free oscillation amplitude that avoids exceeding a critical contact stress to minimize tip/sample damage. With this the measured time delay of the AFM controller system only is 40 ns. However, the additional delays of the high voltage amplifier, z-actuator, and cantilever itself need to be considered to estimate the total delay time of the system.

IV. SCANNING PROBES IN NANOSTRUCTURE FABRICATION

Advantages of SPL methods comprise resolution that approaches the atomic level, for both AFM and STM techniques, the ability to produce features with nearly arbitrary geometries, and the capability to pattern over surface topography that deviates significantly from planarity. However, scanning probe based methods are limited by their serial processing scheme, which limits the throughput in both writing and imaging mode of the system. Increasing the throughput could be achieved by (1) improvement of the writing and imaging speed, (2) the scaling up of the physical process by cantilever array technology based on a thermally driven self-sensing probe concept, and (3) by combination of different lithographic methods in a mix and match lithography approach.[12] Unless these approaches yield a huge increase in throughput, it is likely that SPL methods will be applied for rapid nanoscale prototyping and critical dimension patterning, wherein ultra-high resolution and overlay alignment capabilities are required, or patterning of master templates for high resolution NIL.

The flexibility inherent in scanning probe techniques offers broad possibilities for SPL-based fabrication and analysis nanoelectronic and nanomechanical devices. To move beyond the state of the art unique nanofabrication capabilities the following expectations must be considered to enable sustainable single nanometer manufacturing: (1) The generation, placement, overlay alignment, and inspection of the lithographic nanostructures must be accomplished in a precise, reproducible, controlled, and sustainable manner. (2) The SPL cantilever has to be very small allowing high speed "writing" and "reading" (Figs. 2–6). (3) SPL-tips must keep their specifications over their expected tip lifetimes (tip-wear). (4) SPL must be scalable up to the required throughput and yield.[21,38]

Recently, we have demonstrated the positive-tone, developmentless, so called "self-development" patterning of calixarene molecular glass resists using highly confined electric field, current-controlled scanning probe lithography (EF-CC-SPL) scheme.[6,7,38,39] Herein, an electric field is applied between scanning probe and sample, resulting in a current flux of low energy electrons (<50 eV), which is regulated by the lithography current feedback loop. This current flux in turn penetrates the molecular resist material below the nanoprobe, leading to a highly localized removal process used for patterning of nanofeatures. In Figs. 10 and 11, the basic principle of the SPL system using thermally actuated, piezoresistive cantilever with conductive tip is summarized. It is a closed loop SPL system modifying calixarene-based molecular glass resists.

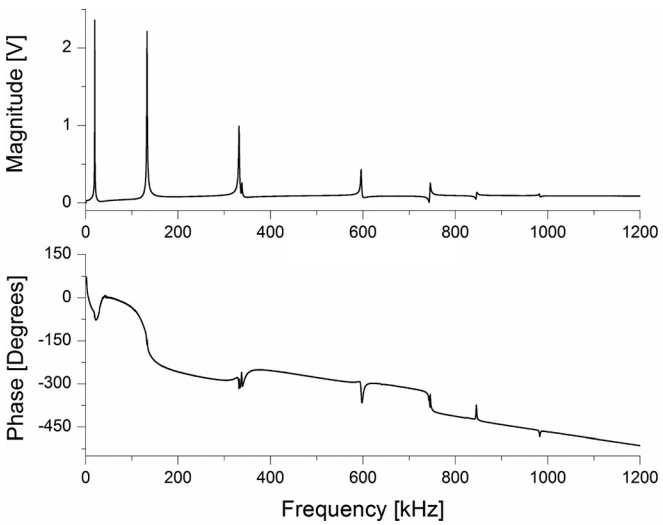

FIG. 9. Sinusoidal frequency sweep (magnitude and phase vs frequency plot) shows seven resonant modes of an active cantilever. Excitation of the cantilever is provided with a bimaterial thermally driven microheater and read-out by an integrated piezoresistive sensor bridge.

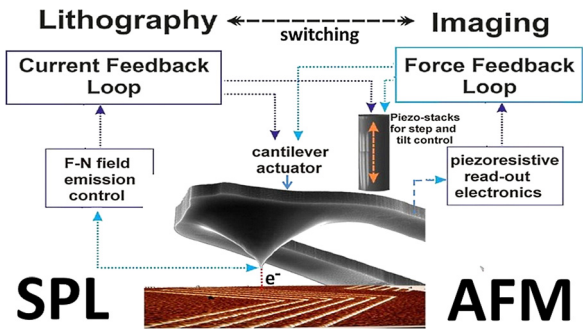

FIG. 10. (Color online) Schematic layout of the lithography system incorporating a current feedback loop for SPL and a force feedback loop for AFM imaging and probing. Between both modes (imaging and lithography) could be switched, indicated by the dotted double arrow. Thus, the same nanoprobe is used for both (a) direct writing of nanofeatures using spatially confined low-energy electron emission from nanoprobe-tip and (b) AFM-imaging for pre- and postinspection as well as for pattern overlay alignment (Ref. 39).

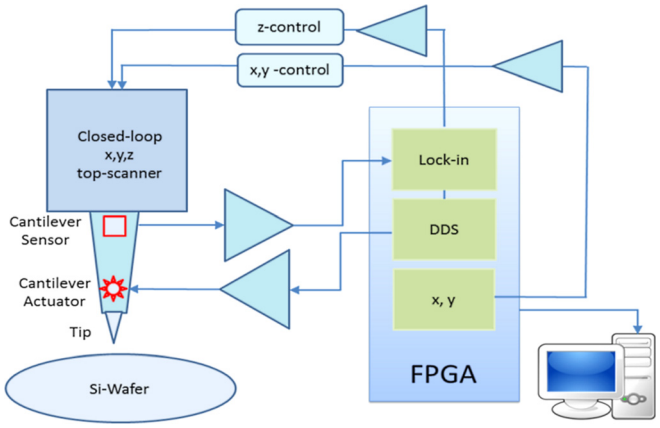

FIG. 11. (Color online) Block diagram of the AFM and distance control feedback loop for an active cantilever (self-actuating, self-sensing) and a top-scanner system.

In Figs. 12 and 13, high fidelity lithographic results are shown achieved with the EF-CC-SPL scheme. AFM imaging of the patterns was carried out directly after SPL in closed loop fashion[39] using the same cantilever as for imaging. In Fig. 12, fine corner features composed of single lines are patterned at a fixed half pitch of 250 nm, whereas in Fig. 13, the half pitch within each single meander line feature was modulated from (1) 75 nm, (2) 50 nm down to (3) 25 nm and backward. Each meander line was patterned with different exposure parameters, whereby Fig. 13(b) was underexposed, Fig. 13(d) was overexposed, and the features in Figs. 13(a) and 13(c) were exposed at optimum dose demonstrating high fidelity pattern. A more detailed description of the line-width dependencies from bias voltage, exposure dose and tip is provided elsewhere.[6,7] In summary, the self-developing EF-CC-SPL scheme offers a high resolution mask-less patterning method (sub-5 nm lines[12]) applicable for a closed loop SPL strategy. Herein, we have recently demonstrated the promising combination of EF-CC-SPL with electron beam lithography (also extreme ultraviolet lithography is possible instead) in a mix-and-match approach,[12] increasing both the process window and the throughput of the EF-CC-SPL method.

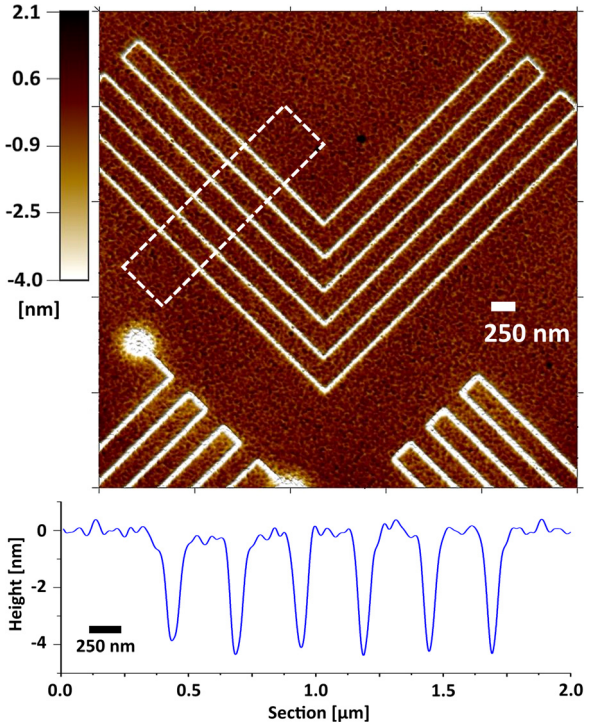

FIG. 12. (Color online) AFM topography 2D image of fine corner line features written into 5 nm thick calixarene resist (non-deconvoluted image, scale bar: 250 nm, area averaged for section graph marked by dotted rectangle). AFM-imaging was carried out after SPL in closed-loop fashion using the same cantilever as for lithography (7 nm tip radius of curvature).

Figure 11 shows a block diagram of the AFM setup used, controlled by a FPGA system. A low amplitude oscillation of the cantilever near the sample surface is driven through the bimaterial thermal actuator and the deflection tracked with the piezoresistive read-out as described previously. In the case of AM operation, the drive signal was generated by a signal of the direct digital synthesizer, which can be set to the frequencies of the first or higher eigenmodes of the cantilever, respectively. The amplitudes and phase shifts for each eigenmode can be captured by the lock-in amplifiers. However, in most scanning probe microscopes, throughput

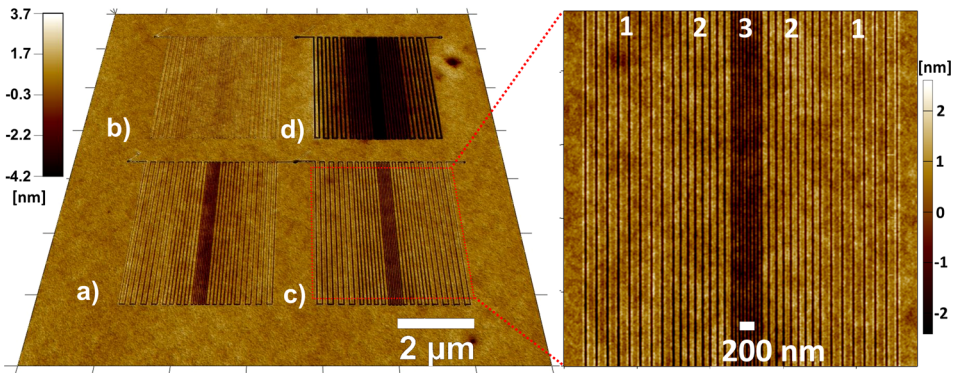

FIG. 13. (Color online) AFM topography images (3D overview image, scale bar: 2 μm; 2D zoom-in image, scale bar: 200 nm) of long meander line features patterned into 10 nm thick calixarene resist (non-deconvoluted image). AFM imaging was carried out directly after SPL processing (no step in between) using the same cantilever (5 nm tip radius of curvature). The meander features were patterned at 30 V bias voltage, whereby the line exposure dose was modulated from (a) 100 nC/cm; (b) 66.7 nC/cm; (c) 133.3 nC/cm; (d) 400 nC/cm, respectively. Within each meander line the line pitch was modulated from (1) 75 nm hp; (2) 50 nm hp; (3) 25 nm hp, and backward.

is limited by the speed at which the cantilever-tip can be moved over the sample surface. For constant force imaging this speed is commonly limited by the speed of the closed-loop system, which is in sequence limited by the speed, or resonance frequency, of the z-axis actuator.

Diverse actuator types for direct cantilever actuation, using an electrostatic-actuator[40] or a piezoelectric thin film,[41] have been developed. As was demonstrated with the European Project "Pronano,"[11] by integrating a bimaterial thermally driven actuator[29] on a cantilever equipped with a piezoresistive read-out, the scan speed of an AFM can be increased by an order of magnitude over the standard AFM. The throughput of the scanning probe microscope system has been enhanced by using parallel cantilever arrays, and by increasing the deflection bandwidth of each probe individually. The main advantage of the bimaterial thermally driven actuator on the cantilever is not only excite the cantilever in its resonance but also deflect the cantilever at lower frequencies off-resonance (1 Hz–10 kHz). When a DC-current is applied to the microheater, the cantilever bends proportionally to the square of the input current.[30] With such sensors and actuators integrated onto the cantilever, the AFM can be made much smaller since the laser and photodetector alignment are no longer necessary. This enables the build-up of a table-top scanning probe nanolithography system.

V. SUMMARY AND CONCLUSIONS

Fabricating future devices for nanoelectronics, nanophotonics, and nanoelectromechanical systems requires lithography at the single nanometer level. An SPL approach may be essential to create the "beyond CMOS" generation of electronic devices. Over the coming year's sustainable lithographic principles for reproducible sub-5 nm manufacturing of nanostructures will be established to make the SPL the concept of choice. To address this, a high throughput technology using a combination of high resolution SPL and NIL for mass device fabrication has to be considered.

The self-actuated piezoresistive cantilever allows for easier system integration and significant reduction in its weight. Hence, the microscope provides better controllability and significant higher scan speeds, with the potential for full lithographic and metrological automation. For SPL, the implemented AFM-mode is enabling an *in-situ* inspection capability, a quantitative mapping at unprecedented resolution as well as an integrated overlay alignment system.

As with most scientific developments the technological impact of the SPL is difficult to predict. The history of the AFM is a good example for that. New patterning technologies have to be competitive with today's industry's enormous investments. In any case, the properties of novel devices may turn out to be valuable.

ACKNOWLEDGMENT

This project has received funding from the European Union's Seventh Framework Programme for research, technological development and demonstration under Grant Agreement No. [318804] [Single Nanometer Manufacturing for beyond CMOS devices (SNM)].

[1]M. A. Reed, Sci. Am. **268**, 118 (1993).
[2]J. S. C. Kilby, ChemPhysChem **2**, 482 (2001).
[3]J. J. Pla, K. Y. Tan, J. P. Dehollain, W. H. Lim, J. J. L. Morton, D. N. Jamieson, A. S. Dzurak, and A. Morello, Nature **489**, 541 (2012).
[4]K. K. Likharev, Proc. IEEE **87**, 606 (1999).
[5]W. Zhang, A. Thiess, P. Zalden, R. Zeller, P. H. Dederichs, J.-Y. Raty, M. Wuttig, S. Blügel, and R. Mazzarello, Nat. Mater. **11**, 952 (2012).
[6]M. Kaestner and I. W. Rangelow, J. Vac. Sci. Technol., B **29**, 06FD02 (2011).
[7]M. Kaestner and I. W. Rangelow, Microelectron. Eng. **97**, 96 (2012).
[8]K. Wilder, H. T. Soh, A. Atalar, and C. F. Quate, J. Vac. Sci. Technol., B **15**, 1811 (1997).
[9]C. R. K. Marrian and D. M. Tennant, J. Vac. Sci. Technol., A **21**, 207 (2003).
[10]K. Ivanova *et al.*, J. Vac. Sci. Technol., B **26**, 2367 (2008).
[11]T. Sulzbach and I. W. Rangelow, PRONANO: *Proceedings of the Integrated Project on Massively Parallel Intelligent Cantilever Probe Platforms for Nanoscale Analysis and Synthesis*, Monsenstein und Vannerdat, Auflage (2010), p. 1.
[12]M. Kaestner, M. Hofer, and I. W. Rangelow, J. Micro/Nanolithogr., MEMS, MOEMS **12**, 031111 (2013).
[13]P. Vettiger *et al.*, IEEE Trans. Nanotechnol. **1**, 39 (2002).
[14]D. A. Walters, J. P. Cleveland, N. H. Thomson, P. K. Hansma, M. A. Wendman, G. Gurley, and V. Elings, Rev. Sci. Instrum. **67**, 3583 (1996).
[15]Y. L. Lyubchenko, S. L. Shlyakhtenko, and T. Ando, Methods **54**, 274 (2011).
[16]T. Sulchek, G. G. Yaralioglu, C. F. Quate, and S. C. Minne, Rev. Sci. Instrum. **73**, 2928 (2002).
[17]T. Sulchek, R. Hsieh, J. D. Adams, G. G. Yaralioglu, S. C. Minne, C. F. Quate, J. P. Cleveland, A. Atalar, and D. M. Adderton, Appl. Phys. Lett. **76**, 1473 (2000).
[18]J. Fleming, B. J. Kenton, and K. K. Leang, Ultramicroscopy **110**, 1205 (2010).
[19]M. B. Viani, T. E. Schaffer, A. Chand, M. Rief, H. E. Gaub, and P. K. Hansma, J. Appl. Phys. **86**, 2258 (1999).
[20]N. Vorbringer-Doroshovets *et al.*, Proc. SPIE **8680**, 868018 (2013).
[21]G. Binnig, U.S. Patent No. 4,724,318 (4 August 1986).
[22]G. Binnig, C. F. Quate, and C. Gerber, Phys. Rev. Lett. **56**, 930 (1986).
[23]G. Binnig, H. Rohrer, C. Gerber, and E. Weibel, Appl. Phys. Lett. **40**, 178 (1982).
[24]M. Tortonese, R. C. Barrett, and C. F. Quate, Appl. Phys. Lett. **62**, 834 (1993).
[25]I. W. Rangelow, S. Skocki, and P. Dumania, Microelectron. Eng. **23**, 365 (1994).
[26]T. Gotszalk, P. Grabiec, and I. W. Rangelow, Ultramicroscopy **82**, 39 (2000).
[27]I. W. Rangelow, F. Shi, P. Hudek, T. Gotszalk, P. B. Grabiec, and P. Dumania, Proc. SPIE **2879**, 56 (1996).
[28]E. I. Givargizov, A. N. Stepanova, E. S. Mashkova, V. A. Molchanov, M. E. Givargizov, and I. W. Rangelow, Ultramicroscopy **82**, 57 (2000).
[29]I. W. Rangelow, Microelectron. Eng. **83**, 1449 (2006).
[30]T. Ivanov, T. Gotszalk, T. Sulzbach, and I. W. Rangelow, Ultramicroscopy **97**, 377 (2003).
[31]T. Michels and I. W. Rangelow, Microelectron. Eng. **126**, 191 (2014).
[32]R. Pedrak *et al.*, J. Vac. Sci. Technol., B **21**, 3102 (2003).
[33]Y. Kanda, IEEE Trans. Electron Devices **29**, 64 (1982).
[34]A. A. Barlian, W. T. Park, J. R. Mallon, A. J. Rastegar, and B. L. Pruitt, Proc. IEEE **97**, 513 (2009).
[35]T. Gotszalk, D. Kopiec, A. Sierakowski, P. Janus, P. Grabiec, and I. W. Rangelow, Proc. SPIE **9236**, 92360A (2014).
[36]I. W. Rangelow, J. Vac. Sci. Technol., A **21**, 1550 (2003).
[37]G. Jozwiak, D. Kopiec, P. Zawierucha, T. Gotszalk, P. Janus, P. Grabiec, and I. W. Rangelow, Sens. Actuators, B **170**, 201 (2012).
[38]I. W. Rangelow, T. Ivanov, Y. Sarov, A. Schuh, A. Frank, H. Hartmann, J.-P. Zollner, D. Olynick, and V. Kalchenko, Proc. SPIE **7637**, 76370V (2010).
[39]M. Kaestner and I. W. Rangelow, Proc. SPIE **8323**, 83231G (2012).
[40]J. Malo and J. I. Izpura, Sens. Actuators, A **136**, 347 (2007).
[41]S. R. Manalis, S. C. Minne, and C. F. Quate, Appl. Phys. Lett. **68**, 871 (1996).